

LEARNING AUDIO-VISUAL REPRESENTATIONS WITH ACTIVE CONTRASTIVE CODING

Shuang Ma

Microsoft
Redmond, WA, USA

Zhaoyang Zeng

Sun Yat-sen University
Guangzhou, China

Daniel McDuff

Microsoft Research
Redmond, WA, USA

Yale Song

Microsoft Research
Redmond, WA, USA

ABSTRACT

Contrastive coding has achieved promising results in self-supervised representation learning. However, there are practical challenges given that obtaining a tight lower bound on mutual information (MI) requires a sample size exponential in MI and thus a large set of negative samples. We can incorporate more samples by building a large queue-based dictionary, but there are theoretical limits to performance improvements even with a large number of negative samples. We hypothesize that *random negative sampling* leads to a highly redundant dictionary, which could result in representations that are suboptimal for downstream tasks. In this paper, we propose an active contrastive coding approach that builds an *actively sampled* dictionary with diverse and informative items, which improves the quality of negative samples and achieves substantially improved results on tasks where there is high mutual information in the data, e.g., video classification. Our model achieves state-of-the-art performance on multiple challenging audio and visual downstream benchmarks including UCF101, HMDB51 and ESC50.

1 INTRODUCTION

Recent studies have demonstrated promising results on contrastive learning of audio and visual representations (Oord et al., 2018; Hénaff et al., 2019; Schneider et al., 2019; Chen et al., 2020). The self-supervised training process can be understood as building a dynamic dictionary per mini-batch, where “keys” are typically *randomly* sampled from the data. The encoders are trained to perform dictionary look-up: an encoded “query” should be similar to the value of its matching key and dissimilar to others. This training objective maximizes a lower bound of mutual information (MI) between representations and the data (Hjelm et al., 2018; Arora et al., 2019). However, such lower bounds are tight only for sample sizes exponential in the MI (McAllester & Stratos, 2020), suggesting the importance of building a large and consistent dictionary across mini-batches.

Consequently, He et al. (2020) designed Momentum Contrast (MoCo) that builds a queue-based dictionary with momentum updates. It decouples the dictionary size from the memory capacity of modern GPUs/TPUs, and thus practically achieves a large and consistent dictionary. However, Arora et al. (2019) showed that simply increasing the dictionary size beyond a threshold does not improve (and sometimes can even harm) the performance on downstream tasks. Furthermore, we find that MoCo can suffer when there is high redundancy in the data, because only relevant – and thus limited – parts of the dictionary are updated in each iteration, ultimately leading to a dictionary of redundant items (we show this empirically in Fig. 3). We argue that *random negative sampling* is much responsible for such theoretically and empirically validated issue: a randomly constructed dictionary will contain more “biased keys” (similar keys that belong to the same class) and “ineffective keys” (keys that can be easily discriminated by the current model) than a carefully constructed one. Furthermore, this issue can get aggravated when the dictionary size is large.¹

In this paper, we focus on learning audio-visual representations of video data by leveraging the natural correspondence between the two modalities, which serves as a useful self-supervisory signal

¹Fig. 2 blue lines show the probability of sampling unique negatives (instances from different categories) decreases from 37.5% to 30.8% when we increase the batch size from 32 to 128. We compute the probabilities by averaging the number of unique categories across iterations and dividing them by their batch size.

(Owens & Efros, 2018; Owens et al., 2016; Alwassel et al., 2019). Our starting point is contrastive learning (Gutmann & Hyvärinen, 2010; Oord et al., 2018) with momentum updates (He et al., 2020). However, as we discussed above, there are both practical challenges and theoretical limits to the dictionary size. This issue is common to all natural data but is especially severe in video; successive frames contain highly redundant information, and from the information-theoretic perspective, audio-visual channels of video data contain higher MI than images because the higher dimensionality – i.e., temporal and multimodal – reduces the uncertainty between successive video clips. Therefore, a dictionary of *randomly sampled* video clips would contain highly redundant information, causing the contrastive learning to be ineffective. Therefore, we propose an *actively sampled* dictionary to sample informative and diverse set of negative instances. Our approach is inspired by active learning (Settles, 2009) that aims to identify and label only the maximally informative samples, so that one can train a high-performing classifier with minimal labeling effort. We adapt this idea to construct a non-redundant dictionary with informative negative samples.

Our proposed approach, Cross-Modal Active Contrastive Coding (CM-ACC), learns discriminative audio-visual representations from unlabeled videos and achieves substantially better results on video data with a high amount of redundancy (and thus high MI). We demonstrate our approach through various ablation studies and comparisons to several state-of-the-art methods. We show that our *actively sampled* dictionary contains negative samples from a wider variety of semantic categories than a randomly sampled dictionary. As a result, our approach can benefit from large dictionaries even when randomly sampled dictionaries of the same size starts to deteriorate the model performance. When pretrained on AudioSet (Gemmeke et al., 2017), our approach achieves new state-of-the-art classification performances on UCF101 (Soomro et al., 2012), HMDB51 (Kuehne et al., 2011), and ESC50 (Piczak, 2015b), outperforming models trained even in a fully-supervised manner.

2 BACKGROUND

Our work builds upon the recent progress on contrastive representation learning (Gutmann & Hyvärinen, 2010; Oord et al., 2018) and especially the momentum contrast approach (He et al., 2020). Below we provide their core concepts and discuss recent theoretical studies on the limitations of contrastive learning (Arora et al., 2019; McAllester & Stratos, 2020).

Contrastive Learning. Gutmann & Hyvärinen (2010); Oord et al. (2018); Hénaff et al. (2019) learn the representation of data by comparing encoded representations of similar samples with dissimilar ones (called “negative samples”) drawn from the same data distribution. This is often formulated as a cross-entropy loss with the learning objective that forces the representations of similar samples to be more similar to each other than with negative samples:

$$\min_{\theta_f, \theta_h} \mathbb{E}_{x \sim p_{\mathcal{X}}} \left[-\log \left(\frac{e^{f(x; \theta_f)^\top h(x^+; \theta_h)}}{e^{f(x; \theta_f)^\top h(x^+; \theta_h)} + e^{f(x; \theta_f)^\top h(x^-; \theta_h)}} \right) \right] \quad (1)$$

where $f(\cdot)$ and $h(\cdot)$ are feature encoders with learnable parameters θ_f and θ_h , respectively. The samples x^+ and x^- are drawn from the same distribution as $x \in \mathcal{X}$, and are assumed to be similar and dissimilar to x , respectively. Minimizing this objective encourages $f(\cdot)$ and $h(\cdot)$ to learn discriminative representations of x such that (x, x^+) have a higher similarity than all the other pairs of (x, x^-) . The similarity in this case is measured by the dot product between representations, but other metrics can also be used, e.g., the log-bilinear form (Oord et al., 2018).

We can interpret the contrastive learning objective as a dynamic dictionary look-up process. Given a “query” x , it finds the correct “key” x^+ among the other irrelevant keys x^- in a dictionary. In this perspective, the optimal solution to equation 1 will enable a dictionary look-up of x^+ given a query x . Denoting the query by $q = f(x)$, the correct key by $k^+ = h(x^+)$, and the dictionary of K negative samples by $\{k_i = h(x_i)\}, i \in [1, K]$, we can express equation 1 in a softmax form,

$$\min_{\theta_q, \theta_k} \mathbb{E}_{x \sim p_{\mathcal{X}}} \left[-\log \frac{e^{q \cdot k^+ / \tau}}{\sum_{i=0}^K e^{q \cdot k_i / \tau}} \right] \quad (2)$$

where θ_q and θ_k are parameters associated with the query and key encoders, respectively, and τ is a temperature term that controls the shape of the probability distribution computed by the softmax

function. Assuming there is a single positive key k^+ in the dictionary, the above objective can be seen as a $(K + 1)$ -way softmax classifier that aims to classify q as k^+ .

Momentum Contrast (MoCo). The standard approach to contrastive learning builds a dictionary dynamically per mini-batch (Oord et al., 2018; Hénaff et al., 2019); the $(K + 1)$ samples correspond to a mini-batch of one positive and K negative samples, which are often randomly chosen from the dataset. This is convenient as we can update the entire model parameters by the standard back-propagation; Fig. 1(a) illustrates this standard approach. However, this approach couples the dictionary size to the mini-batch size, which is capped by the GPU/TPU capacity.

MoCo (He et al., 2020) decouples the dictionary size with the mini-batch size by implementing a queue-based dictionary, i.e., current mini-batch samples are enqueued while the oldest are dequeued. It then applies momentum updates to parameters of a key encoder θ_k with respect to parameters of a query encoder, $\theta_k \leftarrow m\theta_k + (1 - m)\theta_q$, where $m \in [0, 1)$ is a momentum coefficient. Only the parameters θ_q are updated by back-propagation, while the parameters θ_k are defined as a moving average of θ_q with exponential smoothing. These two modifications allow MoCo to build a large and slowly-changing (and thus consistent) dictionary, which lead to substantial improvements on various image recognition tasks including classification, detection, and segmentation (He et al., 2020).

Theoretical Limitations of Contrastive Learning. Recent work provides theoretical analysis on the shortcomings of contrastive learning. McAllester & Stratos (2020) show that lower bounds to the MI are only tight for sample size exponential in the MI, suggesting that a large amount of data are required to achieve a tighter lower bound on MI. He et al. (2020) empirically showed that increasing negative samples has shown to improve the learned presentations. However, Arora et al. (2019) showed that such a phenomenon does not always hold: Excessive negative samples can sometimes hurt performance. Also, when the number of negative samples is large, the chance of sampling redundant instances increases, limiting the effectiveness of contrastive learning. One of our main contributions is to address this issue with active sampling of negative instances, which reduces redundancy and improves diversity, leading to improved performance on various downstream tasks.

3 APPROACH

We present cross-modal active contrastive coding (CM-ACC) to learn audio-visual representations from unlabeled videos. Fig. 1 highlights the main idea of our approach.

3.1 CROSS-MODAL CONTRASTIVE REPRESENTATION LEARNING

Let $A = \{a_0, \dots, a_{N-1}\}$ and $V = \{v_0, \dots, v_{N-1}\}$ be collections of audio and visual clips, where each pair (a_i, v_i) is taken from the same block of a video and temporally synchronized, for all $i \in [0, N)$. We define query encoders f_a and f_v and key encoders h_a and h_v for audio and visual clips, respectively, with learnable parameters $\{\theta_q^a, \theta_q^v\}$ for the query encoders and $\{\theta_k^a, \theta_k^v\}$ for the key encoders. These encoders compute representations of audio and visual clips as queries and keys,

$$q^v = f_v(v^{query}), \quad k^v = h_v(v^{key}), \quad q^a = f_a(a^{query}), \quad k^a = h_a(a^{key}) \quad (3)$$

We propose a cross-modal contrastive predictive coding scheme that leverages the natural correspondence between audio and visual channels of video data. At a high-level, our learning objective encourages the representations of audio and visual clips to be similar if they come from the same temporal block of a video. Fig. 1(b) illustrates our cross-modal predictive coding setup.

We train our encoders to perform cross-modal dictionary look-up: Taking as an example the visual-to-audio predictive coding scenario, given a query video clip v^{query} , we want to find the corresponding audio clip a^{key} from a dictionary D_a . Extending MoCo (He et al., 2020) to our cross-modal setup, we implement a queue-based dictionary D_a that stores keys of audio clips $\{k_i^a\}_{i=1}^K$, where K is the dictionary size. We compute the contrastive loss of equation 2 and backpropagate the gradients only to the visual query encoder f_v and update the parameters θ_q^v . For the audio encoder h_a , we apply the momentum update (He et al., 2020),

$$\theta_k^a \leftarrow m\theta_k^a + (1 - m)\theta_q^a \quad (4)$$

Note that we have not updated θ_q^a in this visual-to-audio predictive coding step; we update it during the audio-to-visual predictive coding step (which follows the same process as above with the op-

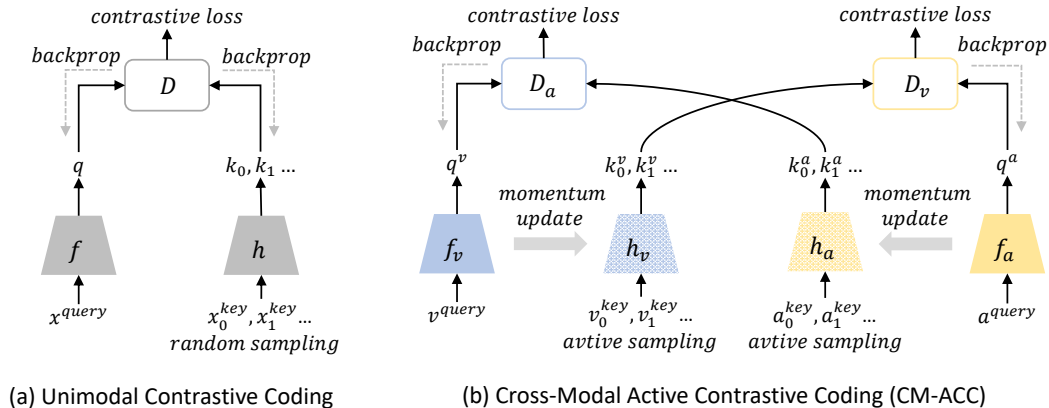


Figure 1: Our approach (b) extends contrastive coding (a) to the cross-modal scenario and adapts the momentum contrast (MoCo) (He et al., 2020) to the dictionary update. Different from all existing work, we propose an active learning idea to the negative sampling.

posite order of modalities). Also note that, although we explain the visual-to-audio step only, we perform bi-directional predictive coding and end-to-end train the whole model.

3.2 ACTIVE SAMPLING OF NEGATIVE INSTANCES

The quality of negative samples is crucial in contrastive learning. Existing work in contrastive learning typically adopts random negative sampling. However, we want a diverse set of negative samples in our dictionary so that comparisons between positive and negative pairs are most informative. In the supervised setting, this can be done by sampling instances from different categories than the query instance. Unfortunately, in the unsupervised case we do not have access to the labels.

Motivated by active learning (Settles, 2009), we propose a novel gradient-based active sampling approach to improve the quality of negative samples. In active learning, the learner chooses samples that seem maximally informative and queries an oracle for labels to obtain an optimal solution with a minimal labeling budget. Adapting this to our setting, we can empower the learner to choose the maximally informative negative samples to construct a dictionary; the main question is how to measure the *informativeness* of samples without labels.

One way to measure the informativeness is through the lens of *uncertainty*: If a model is highly uncertain about its prediction of a sample, we can ensure the maximum update to the model by including the sample in a mini-batch (conversely, if the uncertainty is low for all samples in a mini-batch, the model update will be small). In the first-order optimization regime, such as SGD (LeCun et al., 1998) and its variants, Ash et al. (2020) have shown that gradients of a loss function with respect to the model’s most confident predictions can approximate the uncertainty of samples, demonstrating its effectiveness in active learning where ground-truth labels are assumed to be unknown. They provide a theoretical justification by showing that gradient norms of the last layer of a neural network with respect to pseudo-labels provides a lower bound on gradient norms induced by any other labels. In this work, we use gradients of the last layer to measure the uncertainty and encourage our model to include samples that have the highest gradient magnitudes to constitute a dictionary.

While the uncertainty of each individual samples is important, the *diversity* of samples is also a critical measure of informativeness. Intuitively, it is possible that a model is highly uncertain about samples from particular semantic categories, but constructing a mini-batch of samples from just those categories can severely bias gradients and ultimately lead to a bad local minima. There are several principled approaches to ensure the diversity of samples, such as submodular optimization (Fujishige, 2005) and Determinantal Point Processes (DPP) (Macchi, 1975; Kulesza & Taskar, 2011). Unfortunately, those methods are computationally heavy because of the combinatorial search space (Nemhauser et al., 1978; Gilks et al., 1995). In this work, instead of using the expensive solutions,

Algorithm 1 Cross-Modal Active Contrastive Coding

```

1: Require: Audio-visual clips  $A, V$ ; dictionaries  $D_a, D_v$ ; encoders  $f_v, f_a, h_v, h_a$ ;
   dictionary size  $K$ ; pool size  $N$ ; mini-batch size  $M$ ; learning rate  $\gamma$ ; momentum  $m$ 
2: Initialize parameters,  $\theta_q^v, \theta_k^v, \theta_q^a, \theta_k^a \sim Uniform(0, 1)$ 
3: Load a random dictionary of visual clips,  $D_v \leftarrow \{v_1, \dots, v_K\} \sim Random(V)$ 
4: Load a random dictionary of audio clips,  $D_a \leftarrow \{a_1, \dots, a_K\} \sim Random(A)$ 
5: Encode dictionary samples,  $k_i^v \leftarrow h_v(v_i), \forall v_i \in D_v, k_i^a \leftarrow h_a(a_i), \forall a_i \in D_a$ 
6: for  $epoch = 1$  to #epochs: do
7:   Load a random pool of visual clips,  $U_v \leftarrow \{v_1, \dots, v_N\} \sim Random(V)$ 
8:   Load a random pool of audio clips,  $U_a \leftarrow \{a_1, \dots, a_N\} \sim Random(A)$ 
9:   Encode pool samples,  $k_n^v \leftarrow h_v(v_n), \forall v_n \in U_v, k_n^a \leftarrow h_a(a_n), \forall a_n \in U_a$ 
10:  for  $t = 1$  to #mini-batches: do
11:    Load a mini-batch of visual clips,  $B_v \leftarrow \{v_1, \dots, v_M\} \sim V$ 
12:    Load a mini-batch of audio clips,  $B_a \leftarrow \{a_1, \dots, a_M\} \sim A$ 
13:     $\triangleright$  Active sampling of negative video keys for  $D_v$ 
14:    Encode mini-batch samples,  $q_i^a \leftarrow f_a(a_i), \forall a_i \in B_a$ 
15:    for  $\forall v_n \in U_v \setminus D_v$ : do
16:      Compute pseudo-posterior,  $p(\hat{y}_n^v | v_n, B_a) \leftarrow \frac{\exp(k_n^v \cdot q_j^a)}{\sum_{i=1}^M \exp(k_n^v \cdot q_i^a)}, \forall j \in [1, M]$ 
17:      Compute pseudo-label,  $\tilde{y}_n^v \leftarrow \arg \max p(\hat{y}_n^v | \cdot)$ 
18:    end for
19:    Compute gradient,  $g_{v_n} \leftarrow \frac{\partial}{\partial \theta_{iast}} \mathcal{L}_{CE}(p(\hat{y}_n^v | \cdot), \tilde{y}_n^v) |_{\theta=\theta_q^a}, \forall n \in [1, N]$ 
20:    Obtain  $S_v \leftarrow k\text{-MEANS}_{\text{INIT}}^{++}(\{g_{v_n} : v_n \in U_v \setminus D_v\}, \#seeds = M)$ 
21:    Update  $D_v \leftarrow \text{ENQUEUE}(\text{DEQUEUE}(D_v), S_v)$ 
22:     $\triangleright$  Active sampling of negative audio keys for  $D_a$ 
23:    Encode mini-batch samples,  $q_i^v \leftarrow f_v(v_i), \forall v_i \in B_v$ 
24:    for  $\forall a_n \in U_a \setminus D_a$ : do
25:      Compute pseudo-posterior,  $p(\hat{y}_n^a | a_n, B_v) \leftarrow \frac{\exp(k_n^a \cdot q_j^v)}{\sum_{i=1}^M \exp(k_n^a \cdot q_i^v)}, \forall j \in [1, M]$ 
26:      Compute pseudo-label,  $\tilde{y}_n^a \leftarrow \arg \max p(\hat{y}_n^a | \cdot)$ 
27:    end for
28:    Compute gradient,  $g_{a_n} \leftarrow \frac{\partial}{\partial \theta_{iast}} \mathcal{L}_{CE}(p(\hat{y}_n^a | \cdot), \tilde{y}_n^a) |_{\theta=\theta_q^v}, \forall n \in [1, N]$ 
29:    Obtain  $S_a \leftarrow k\text{-MEANS}_{\text{INIT}}^{++}(\{g_{a_n} : a_n \in U_a \setminus D_a\}, \#seeds = M)$ 
30:    Update  $D_a \leftarrow \text{ENQUEUE}(\text{DEQUEUE}(D_a), S_a)$ 
31:     $\triangleright$  Cross-modal contrastive predictive coding
32:    Encode mini-batch samples,  $k_i^v \leftarrow h_v(v_i), \forall v_i \in B_v, k_i^a \leftarrow h_a(a_i), \forall a_i \in B_a$ 
33:    Compute the posterior,  $p(y_i^v | v_i, a_i, D_a) = \frac{\exp(q_i^v \cdot k_i^a / \tau)}{\sum_{j=0}^K \exp(q_i^v \cdot k_j^a / \tau)}, \forall i \in [1, M]$ 
34:    Compute the posterior,  $p(y_i^a | a_i, v_i, D_v) = \frac{\exp(q_i^a \cdot k_i^v / \tau)}{\sum_{j=0}^K \exp(q_i^a \cdot k_j^v / \tau)}, \forall i \in [1, M]$ 
35:     $\triangleright$  Update model parameters
36:    Update  $\theta_q^v \leftarrow \theta_q^v - \gamma \nabla_{\theta} \mathcal{L}_{CE}(p(y^v | \cdot), y_{gt}^v) |_{\theta=\theta_q^v}$ 
37:    Update  $\theta_q^a \leftarrow \theta_q^a - \gamma \nabla_{\theta} \mathcal{L}_{CE}(p(y^a | \cdot), y_{gt}^a) |_{\theta=\theta_q^a}$ 
38:    Momentum update  $\theta_k^v \leftarrow m\theta_k^v + (1 - m)\theta_q^v$ 
39:    Momentum update  $\theta_k^a \leftarrow m\theta_k^a + (1 - m)\theta_q^a$ 
40:  end for
41: end for
42: return Optimal solution  $\theta_q^v, \theta_k^v, \theta_q^a, \theta_k^a$ 

```

we opt to the fast solution of Ash et al. (2020) and use the initialization scheme of the k -MEANS++ seeding algorithm (Arthur & Vassilvitskii, 2007) to sample a diverse set of negative samples.

3.3 CROSS-MODAL ACTIVE CONTRASTIVE CODING

Algorithm 1 describes our proposed cross-modal active contrastive coding (for comparison, we also provide a version without active sampling in Appendix). At a high-level, we initialize the dictionaries D_v and D_a with K randomly drawn samples from V and A , respectively (lines 3–5). For each epoch, we construct “negative candidate pools” U_v and U_a with N random samples from V and A , respectively (lines 7–9). For each iteration within an epoch, we *actively* select the most informative negative samples S_v and S_a from the pools U_v and U_a , respectively, and enqueue them into the dictionaries D_v and D_a , respectively (lines 11–30). We then perform cross-modal con-

trastive predictive coding, update the parameters of query encoders θ_q^v and θ_q^a via backpropagation, and apply momentum updates to the parameters of key encoders θ_k^v and θ_k^a (lines 32–39).

Active sampling. Our sampling approach finds the most informative negative instances by considering both *uncertainty* and *diversity*. To measure the uncertainty, we define a pseudo-label space induced by the queries from the other modality, and take the gradient of the last layer of a query encoder network with respect to the most confident prediction, which we call the pseudo-label \tilde{y} .

For instance, in the case of sampling negative video keys from the pool U_v (lines 14–21), we compute the pseudo-posterior of a video key $v_n \in U_v \setminus D_a$,

$$p(\hat{y}_n^v | v_n, B_a) = \frac{\exp(k_n^v \cdot q_j^a)}{\sum_{i=1}^M \exp(k_n^v \cdot q_i^a)}, \forall j \in [1, M] \quad (5)$$

where B_a is the current mini-batch of audio queries and defines the pseudo-label space. Note that we consider only the samples in $U_v \setminus D_v$ to rule out samples already in D_v . Intuitively, this computes the posterior by the dot-product similarity between v_n and all $q_i^a \in B_a$, producing an M -dimensional probability distribution. We then take the most confident class category as the pseudo-label \tilde{y}_n^v (line 17) and compute the gradient according to the cross-entropy loss

$$g_{v_n} = \frac{\partial}{\partial \theta_{last}} \mathcal{L}_{CE}(p(\hat{y}_n^v | v_n, B_a), \tilde{y}_n^v) |_{\theta=\theta_q^a} \quad (6)$$

where θ_{last} is the parameters of the last layer of θ (in this case, θ_q^a of the audio query encoder h_a). Intuitively, the gradient g_{v_n} measures the amount of change (and thus, the uncertainty) v_n will bring to the audio query encoder h_a .

One can interpret this as a form of *online hard negative mining*: The gradient is measured with respect to the most probable pseudo-label \tilde{y}_n^v induced by the corresponding audio query q_j^a . When we compute the contrastive loss, the same audio query will be maximally confused by v_n with its positive key v^+ per dot-product similarity, and v_n in this case can serve as a hard negative sample.

Next, we obtain the most diverse and highly uncertain subset $S_v \subseteq U_v \setminus D_v$ using the initialization scheme of k -MEANS⁺⁺ (Arthur & Vassilvitskii, 2007) over the gradient embeddings g_v (line 20). The k -MEANS⁺⁺ initialization scheme finds the seed cluster centroids by iteratively sampling points with a probability in proportion to their squared distances from the nearest centroid that has already been chosen (we provide the exact algorithm in the appendix). Intuitively, this returns a *diverse* set of instances sampled in a greedy manner, each of which has a high degree of *uncertainty* measured as its squared distances from other instances that have already been chosen. Finally, we enqueue S_v into D_v and dequeue the oldest batch from D_v (line 21). We repeat this process to sample negative audio keys (lines 23–30); this concludes the active sampling process for D_v and D_a .

Cross-modal contrastive coding. Given the updated D_v and D_a , we perform cross-modal contrastive coding. For visual-to-audio coding, we compute the posteriors of all the video samples $v_i \in B_v$ with respect to the negative samples in the audio dictionary D_a

$$p(y_i^v | v_i, a_i, D_a) = \frac{\exp(q_i^v \cdot k_i^a / \tau)}{\sum_{j=0}^K \exp(q_i^v \cdot k_j^a / \tau)}, \forall i \in [1, M] \quad (7)$$

where the posterior is defined over a cross-modal space with one positive and K negative pairs (line 33). Next, following MoCo (He et al., 2020), we backpropagate the gradient signals only to the query encoders f_v and f_a (lines 36–37), while applying momentum update to the parameters of the key encoders h_v and h_a (lines 38–39). The momentum update allows the dictionaries to change their states slowly, thus making them consistent across iterations.

Note that our momentum update can cause inconsistency in dictionary states because the gradient used to update the query encoders are not directly used to update the corresponding key encoders (see Fig. 1 and lines 38–39 in Alg. 1). To improve the stability during training, we let the gradients flow in a cross-modal fashion (e.g., updating part of f_v and h_a using the same gradient signal from the contrastive loss), by adding one FC layer on top of all encoders and applying momentum update to their parameters. For example, we apply momentum update to the parameters of the FC layer on top of h_a using the parameters of the FC layer from f_v . We omit this in Alg. 1 for clarity but show its importance in our ablation experiments (XMOCO (w/o fcl) in Table 1).

4 RELATED WORK

Self-supervised learning has been extensively studied in vision, language, and audio domains, and several approaches have been proposed on designing new pretext task or more efficient learning objectives. One popular idea in the image domain is learning representations by maximizing the MI (Belghazi et al., 2018; Hjelm et al., 2018). In the video domain, several approaches exploited the underlying structure of video data to design efficient pretext tasks, e.g. by adopting ordering (Sermanet et al., 2017; Wang et al., 2019b), temporal consistency (Dwibedi et al., 2019), and spatio-temporal statistics (Xu et al., 2019; Wang et al., 2019a; Han et al., 2019). In the language domain, the transformer-based approaches trained with the masked language model (MLM) objective has been the most successful (Devlin et al., 2019; Liu et al., 2019; Yang et al., 2019).

Riding on the success of BERT (Devlin et al., 2019), several concurrent approaches generalize it to learn visual-linguistic representations (Lu et al., 2019; Li et al., 2020; Su et al., 2019; Tan & Bansal, 2019; Li et al., 2019). CBT (Sun et al., 2019a) and VideoBERT (Sun et al., 2019b) made efforts on adapting BERT-style pretraining for video. However, the MLM loss requires each token in the sequence to be discrete. The current approaches assume visual representations to be fixed and to be given by pretrained visual encoders (fully-supervised), and define the visual MLM objective in terms of visual similarities (e.g. via vector quantization (VQ) or L2 distance metric) between the original and predicted visual representations. Unfortunately, VQ loses fine-grained information and a pretrained visual encoder limits the learning capacity, which are all crucial for downstream tasks.

Besides vision and language signals, several approaches learn audio-visual representations in a self-supervised manner (Owens et al., 2016; Arandjelovic & Zisserman, 2017; Owens & Efros, 2018; Owens et al., 2016). Recently, audio-visual learning has been applied to enable interesting applications beyond recognition tasks, such as sound source localization/separation (Zhao et al., 2018; Arandjelovic & Zisserman, 2018; Gao et al., 2018; Gao & Grauman, 2019a;b; Ephrat et al., 2018; Gan et al., 2020; Zhao et al., 2019; Yang et al., 2020) and visual-to-sound generation (Hao et al., 2018; Zhou et al., 2018). The work of Owens & Efros (2018), Korbar et al. (2018), and Alwassel et al. (2019) are similar in spirit to our own, but our technical approach differs substantially in the use of active sampling and contrastive learning.

5 EXPERIMENTS

Implementation detail. Unless otherwise noted, we use 3D-ResNet18 (Hara et al., 2018) as our visual encoders (f_v and h_v). For audio encoders (f_a and h_a), we adapt ResNet-18 (He et al., 2016) to audio signals by replacing 2D convolution kernels with 1D kernels. We employ Batch Normalization (BN) (Ioffe & Szegedy, 2015) with the shuffling BN (He et al., 2020) in all our encoders. All models are trained end-to-end with the ADAM optimizer (Kingma & Ba, 2014) with an initial learning rate $\gamma = 10^{-3}$ after a warm-up period of 500 iterations. We use the mini-batch size $M = 128$, dictionary size $K = 30 \times 128$, pool size $N = 300 \times 128$, momentum $m = 0.999$, and temperature $\tau = 0.7$. We used 40 NVIDIA Tesla P100 GPUs for our experiments.

Datasets. We use AudioSet (Gemmeke et al., 2017) and Kinetics-700 (Carreira et al., 2019) as our pretraining data when comparing with state-of-the-art approaches. For Kinetics-700, we use 240K randomly selected videos that contain the audio channel. On AudioSet, we use both a subset of 240K randomly selected videos and the 1.8M full set. For our ablation study, we pretrain our model on Kinetics-Sound (Arandjelovic & Zisserman, 2017) that contains 22K videos from 34 classes of Kinetics that are potentially manifested both visually and audibly. As for downstream tasks, we evaluate our models on action recognition using UCF101 (Soomro et al., 2012) and HMDB51 (Kuehne et al., 2011), and on sound classification using ESC50 (Piczak, 2015b). UCF101 contains 13K video clips from 101 action categories, HMDB51 contains 7K video clips from 51 categories, and ESC50 has 2K audio clips from 50 categories. UCF101 and HMDB51 have 3 official train/test splits, while ESC50 has 5 splits. We conduct our ablation study using `split-1` of each dataset. We report our average performance over all splits when we compare with prior work.

We preprocess video frames by sampling at 10 FPS and applying random cropping, horizontal flipping, gray-scaling, and temporal jittering. We resize video frames to 3-channel images of 224×224 ; we set the clip length to 16 frames during pretraining, and 32 frames during finetuning on downstream tasks. For audio channel, we extract mel-spectrograms from the raw waveform using the

#	Approach	Pretrain Obj.	UCF101	HMDB51	ESC50	Gains
①	Scratch	-	63.3	29.7	54.3	
②	Supervised	Supervised	86.9	53.1	78.3	
③	SMoCo	Uni. rand.	70.7	35.2	69.0	
④	XMoCo (w/o fcl)	Cross rand.	72.9 ($\uparrow 2.2$)	37.5 ($\uparrow 2.3$)	70.9 ($\uparrow 1.9$)	$\Delta(\textcircled{4} - \textcircled{3})$
⑤	XMoCo	Cross rand.	74.1 ($\uparrow 1.2$)	38.7 ($\uparrow 1.2$)	73.0 ($\uparrow 2.1$)	$\Delta(\textcircled{5} - \textcircled{4})$
⑥	CM-ACC	Cross active	77.2 ($\uparrow 3.1$)	40.6 ($\uparrow 1.9$)	79.2 ($\uparrow 6.1$)	$\Delta(\textcircled{6} - \textcircled{5})$

Table 1: Top-1 accuracy of unimodal vs. cross-modal pretraining on downstream tasks.

LibROSA library and get a $80 \times T$ matrix with 80 frequency bands; T is proportionate to the length of an audio clip. We then segment the mel-spectrogram according to the corresponding video clips to ensure temporal synchrony. We treat the mel-spectrograms as an 80-channel 1D signal.

Unimodal vs. cross-modal pretraining. To validate the benefits of cross-modal pretraining, we compare it to its unimodal counterparts. We pretrain our model on Kinetics-Sound with a randomly sampled dictionary (similar to MoCo (He et al., 2020)); we call this XMoCo. For the unimodal case, we pretrain two models on visual clips and audio clips, respectively; we call these SMoCo. We also compare ours with a model trained from scratch (Scratch), and a model pretrained on Kinetics-Sound in a fully-supervised manner (Supervised). Lastly, we include XMoCo (w/o fcl) that is identical to XMoCo except that we do not include the additional FC layers on top of encoders. All these models are finetuned end-to-end on each downstream tasks using the same protocol.

Table 1 shows the top-1 accuracy of each downstream task. We observe that all the self-supervised models outperform Scratch on all downstream tasks, suggesting the effectiveness of pretraining with contrastive learning. We also see that our cross-modal objective outperforms the unimodal objective ($\Delta(\textcircled{4}-\textcircled{3})$). The comparison between XMoCo and XMoCo (w/o fcl) shows the effectiveness of the additional FC layer on top of the encoders ($\Delta(\textcircled{5}-\textcircled{4})$). When adding the FC layer, our performance further improves on all the downstream benchmarks. This shows the importance of letting the gradients flow in a cross-modal fashion. Finally, the performance gap with the full-supervised case shows there are still rooms to improve in self-supervised approaches.

Random vs. active sampling. To validate the benefits of active sampling over random sampling, we compare models pretrained with different sampling approaches on downstream tasks. As shown in Table 1, CM-ACC outperforms the XMoCo, which uses random sampling, by large margins, i.e. 3.1%, 1.9%, and 6.1% on UCF101, HMDB51, and ESC50, respectively ($\Delta(\textcircled{6}-\textcircled{5})$).

Next, we compare the number of unique categories the sampled instances originally belong to, using the ground-truth labels provided in the dataset. The more categories the samples come from, we get more diverse and less redundant samples. We train these on UCF-101 over 300 iterations with different mini-batch sizes, $M \in \{32, 64, 128\}$. Fig. 2 shows that active sampling selects more categories than random sampling across all three mini-batch sizes. At $M = 128$, active sampling

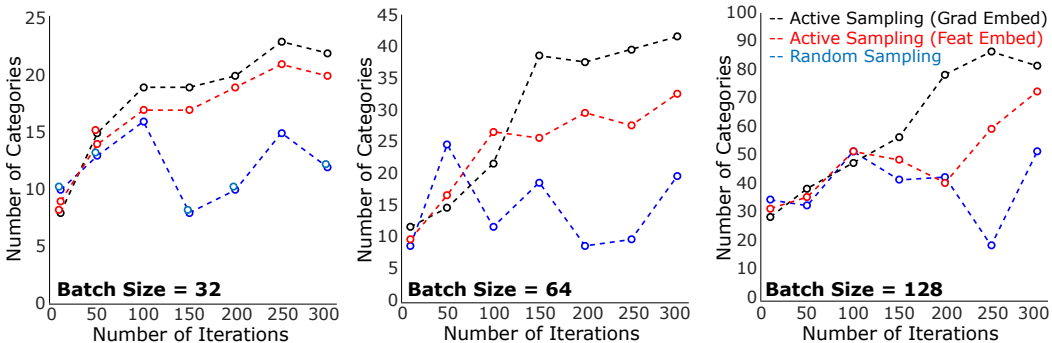


Figure 2: Effects of random sampling and active sampling on the number of categories selected with batch sizes = 32, 64, and 128.

Method	Architecture	Pretrained on (size)	UCF101	HMDB51
Scratch	3D-ResNet18	-	46.5	17.1
Supervised	VGG-M-2048	ImageNet	82.8	46.7
ShuffAL (Misra et al., 2016)	CaffeNet	UCF/HMDB	50.2	18.1
DRL (Buchler et al., 2018)	CaffeNet	UCF/HMDB	58.6	25.0
OPN (Lee et al., 2017)	VGG	UCF/HMDB	59.8	23.8
DPC (Han et al., 2019)	3D-ResNet18	UCF101	60.6	-
MotionPred (Wang et al., 2019a)	C3D	Kinetics400 (N/A)	61.2	33.4
RotNet3D (Jing & Tian, 2018)	3D-ResNet18	Kinetics400 (N/A)	62.9	33.7
ST-Puzzle (Kim et al., 2019)	3D-ResNet18	Kinetics400 (N/A)	65.8	33.7
ClipOrder (Xu et al., 2019)	R(2+1)D-18	Kinetics400 (N/A)	72.4	30.9
CBT (Sun et al., 2019a)	S3D & BERT	Kinetics600 (500K)	79.5	44.6
DPC (Han et al., 2019)	3D-ResNet34	Kinetics400 (306K)	75.7	35.7
SeLaVi (Asano et al., 2020)	R(2+1)D-18	Kinetics400 (240K)	83.1	47.1
AVTS (Korbar et al., 2018)	MC3	Kinetics400 (240K)	85.8	56.9
XDC (Alwassel et al., 2019)	R(2+1)D-18	Kinetics400 (240K)	84.2	47.1
AVID (Morgado et al., 2020)	R(2+1)D-18	Kinetics400 (240K)	87.5	60.8
GDT (Patrick et al., 2020)	R(2+1)D-18	Kinetics400 (N/A)	89.3	60.0
AVTS (Korbar et al., 2018)	MC3	AudioSet (240K)	86.4	-
AVTS (Korbar et al., 2018)	MC3	AudioSet (1.8M)	89.0	61.6
XDC (Alwassel et al., 2019)	R(2+1)D-18	AudioSet (1.8M)	91.2	61.0
AVID (Morgado et al., 2020)	R(2+1)D-18	AudioSet (1.8M)	91.5	64.7
GDT (Patrick et al., 2020)	R(2+1)D-18	AudioSet (1.8M)	92.5	66.1
Ours	3D-ResNet18	UCF101	69.1 (+8.5)	33.3 (+8.3)
	3D-ResNet18	Kine.-Sound (14K)	77.2 (+16.6)	40.6 (+15.6)
	3D-ResNet18	Kinetics700 (240K)	90.2 (+0.9)	61.8 (+1.0)
	3D-ResNet18	AudioSet (240K)	90.7 (+1.4)	62.3 (+1.5)
	3D-ResNet18	AudioSet (1.8M)	94.1 (+1.6)	66.8 (+0.7)
	R(2+1)D-18	AudioSet (1.8M)	93.5 (+1.0)	67.2 (+1.1)

Table 2: Comparison of SOTA approaches on action recognition. We specify pretraining dataset and the number of samples used if they are reported in the original papers (N/A: not available).

(with gradient embedding) covers 60-70% of categories on UCF101, which is substantially more diverse than random sampling (30-40 %). While both sampling schemes perform similarly in early iterations, active sampling starts choosing more diverse instances as the training progresses; this is because the gradient embeddings becomes more discriminative in terms of the uncertainty measure.

Feature vs. gradient embedding. Fig. 2 also compares two ways to do active sampling: using gradient embeddings (Eqn. 6) and feature embeddings (the outputs from h_a and h_v) when selecting the seed centroids with k -MEANS⁺⁺. We see that gradient embeddings results in a more diverse set of negative samples than feature embeddings; this is consistent across all three batch sizes. The gradient embeddings directly measure the uncertainty of each candidate, which is missing from the feature embeddings. This shows the importance of considering both uncertainty and diversity when selecting random samples: the k -MEANS⁺⁺ ensures the diversity in the sample set, but without the uncertainty measure we lose important discriminative information from the candidates.

Effect of dictionary size. Fig. 3 (b) shows how the dictionary size affects downstream task performance. Here we pretrain our model on Kinetics-700 and finetune it on UCF-101. Overall, all three approaches benefit from large dictionaries up to a threshold (at about 10^3), which is consistent with previous empirical findings (He et al., 2020). However, both XMCo and SMCo starts deteriorating performance after about 10^4 (which is consistent with previous theoretical claims of Arora et. al (Arora et al., 2019)), whereas ours do not suffer even after 10^4 . This suggests that there are performance limits by simply increasing the size of a randomly-sampled dictionary, and also shows the benefit of our active sampling approach.

Comparisons with SOTA. Table 3 and Table 2 show the comparison of our approach and existing self-supervised approaches. Table 3 shows that our model outperforms the other SOTA self-supervised models. When comparing with models that trained on medium-size data (Kinetics and AudioSet 240K), our model outperform the top performance (AVID (Morgado et al., 2020) 79.1%) by 0.1% and 1.8% on Kinetics and AudioSet 240K, respectively. Our approach also outperforms

Method	Architecture	Pretrained on (size)	ESC50
Random Forest (Piczak, 2015b)	MLP	ESC50	44.3
Piczak ConvNet (Piczak, 2015a)	ConvNet-4	ESC50	64.5
ConvRBM (Sailor et al., 2017)	ConvNet-4	ESC50	86.5
SoundNet (Aytar et al., 2016)	ConvNet-8	SoundNet (2M+)	74.2
L^3 -Net (Arandjelovic & Zisserman, 2017)	ConvNet-8	SoundNet (500K)	79.3
AVTS (Korbar et al., 2018)	VGG-8	Kinetics (240K)	76.7
XDC (Alwassel et al., 2019)	ResNet-18	Kinetics (240K)	78.0
AVID (Morgado et al., 2020)	ConvNet-9	Kinetics (240K)	79.1
AVTS (Korbar et al., 2018)	VGG-8	AudioSet (1.8M)	80.6
XDC (Alwassel et al., 2019)	ResNet-18	AudioSet (1.8M)	84.8
AVID (Morgado et al., 2020)	ConvNet-9	AudioSet (1.8M)	89.2
GDT (Patrick et al., 2020)	ResNet-9	AudioSet (1.8M)	88.5
Ours	ResNet-18	Kinetics700 (240K)	79.2 (+0.1)
		AudioSet (240K)	80.9 (+1.8)
		AudioSet (1.8M)	90.8 (+1.6)

Table 3: Comparison of SOTA approaches on audio event classification.

the best one (AVID (Morgado et al., 2020) 89.2%) that pretrained on larger-scale dataset (AudioSet 1.8M). Table 2 shows our approach outperforming various self-supervised approaches. To make a fair comparison, we group the SOTA approaches by different pretraining data size, i.e. **small-scale (UCF/HMDB)**, **medium-scale (Kinetics)**, and **large-scale (AudioSet)**. Our gains are calculated with the according counterparts. As we can see, our approach outperform all the other SOTA approaches that pretrained on different dataset and scale. When comparing with GDT (Patrick et al., 2020), the current top model on cross-modal self-supervised learning, our model also outperform it by 1.6 % on UCF101 and 1.1 % on HMDB51. Notably, our approach even outperforms the fully-supervised methods (7.2% on UCF101 and 14.1 % on HMDB51).

6 CONCLUSION

We showed that random sampling could be detrimental to contrastive learning due to the redundancy in negative samples, especially when the sample size is large, and proposed an active sampling approach that yields diverse and informative negative samples. We demonstrated this on learning audio-visual representations from unlabeled videos. When pertained on AudioSet, our approach outperforms previous state-of-the-art self-supervised approaches on various audio and visual downstream benchmarks. We also show that our active sampling approach significantly improves the performance of contrastive learning over random and online hard negative sampling approaches.

A ADDITIONAL EXPERIMENTS

Effect of mutual information. We investigate the impact of the amount of MI on contrastive learning using the Spatial-MultiOmniglot dataset (Ozair et al., 2019). It contains paired images (x, y) of Omniglot characters (Lake et al., 2015) with each image arranged in an $m \times n$ grid (each grid cell is 32×32 pixels). Let l_i be the alphabet size for the i^{th} character in each image, then the MI $I(x, y) = \sum_{i=1}^{mn} \log l_i$. This way, we can easily control the MI by adding or removing characters. We follow the experimental protocol of Ozair et al. (Ozair et al., 2019), keeping the training dataset size fixed at 50K and using the same alphabet sets: Tifinagh (55 characters), Hiragana (52), Gujarati (48), Katakana (47), Bengali (46), Grantha (43), Sanskrit (42), Armenian (41), and Mkhedruli (41).

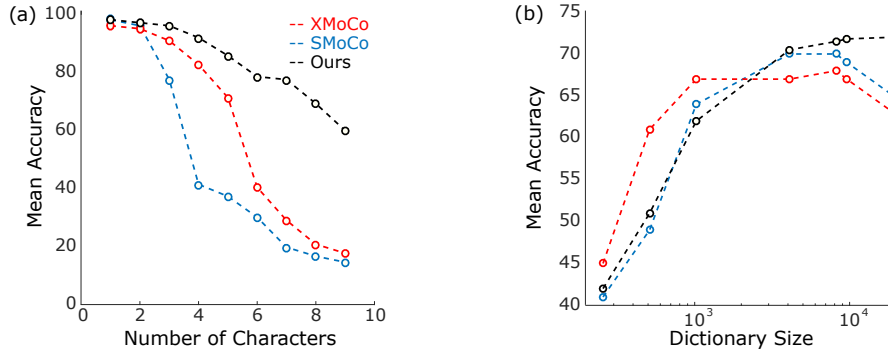


Figure 3: The effect of a) mutual information (Spatial-MultiOmniglot) and b) dictionary size on the accuracy of classification (UCF101).

Fig. 3(a) shows the results as the number of characters (and thus the MI) increases. We see that all approaches achieve nearly 99% accuracy with less than 3 characters; this is the case when the exponent of the MI is smaller than the dataset size (50K), i.e., $e^{I(x,y)} = 55$ with one character, $e^{I(x,y)} = 2,860$ with 2 characters. However, starting from 3 characters, the performance of the regular MoCo (SMoCo) drops significantly; this is because the exponent of the MI ($=137,280$ ($55 \times 52 \times 48$)) is much larger than the dataset size. Although our model also drops performance when the MI is increased, it outperforms the other approaches by a large margin. We also observe that XMoCo outperforms SMoCo in mild conditions (1-5 characters) but performs nearly the same as SMoCo with severe conditions (6-9 characters). This suggests that, while cross-modal prediction helps to learn good representations, it also suffers with the same issue when the MI is large, thus adopting active sampling is beneficial.

Effect of pretraining datasets. We investigate the effects of the pretraining datasets, using Kinetics-Sound (22k), Kinetics (240K), and AudioSet (1.8M). To do this in a controllable manner, we vary pretraining conditions while using the same protocol to finetune the models end-to-end on downstream tasks. Table 4 shows that our model benefits from pretraining on video data, and that the performance improves as we use a large pretraining video dataset (Kinetics and AudioSet) than the relatively smaller dataset (Kinetics-Sound). Notably, our approach even outperforms the fully-supervised pretraining approaches by pretraining on a larger video dataset (1.0%, 3.6%, and 8.5% improvement on UCF101, HMDB51, and ESC50, respectively.)

Approach	Dataset	UCF101	HMDB51	ESC50
Supervised	ImageNet (1.2M)	82.8	46.7	–
	Kinetics-Sound (22K)	86.9	53.1	78.3*
	Kinetics400 (240K) [†]	93.1	63.6	82.3*
CM-ACC	Kinetics-Sound (22K)	77.2	40.6	77.3
	Kinetics700 (240K)	90.2 (-2.9)	61.8 (-1.8)	79.2 (-3.1)
	AudioSet (1.8M)	94.1 (+1.0)	67.2 (+3.6)	90.8 (+8.5)

Table 4: Top-1 accuracy of CM-ACC pretrained on different datasets vs. fully-supervised counterparts (Supervised). * notates the results are implemented by ourselves.

Online hard example mining vs. active sampling. Hard negative mining is used in a variety of tasks, such as detection (Li et al., 2020), tracking (Nam & Han, 2016), and retrieval (Faghri et al., 2017; Pang et al., 2019), to improve the quality of prediction models by incorporating negative examples that are more difficult than randomly chosen ones. As mentioned in the main paper, our active sampling approach can also be interpreted as a form of hard negative mining, in that we actively choose negative samples by optimizing for *uncertainty* and *diversity*.

In this experiment, we compare our approach to online hard example mining (OHEM) (Shrivastava et al., 2016), which constructs negative samples by explicitly choosing the ones that incur high loss values. Specifically, we compute the pseudo-labels for all keys (negative sample candidates) with a given mini-batch of queries. We then compute the classification loss based on these pseudo labels and select the top M keys with the highest loss values. We pretrain the models on Kinetics-700 (Kay et al., 2017) and report the top-1 accuracy on UCF101 (Soomro et al., 2012) and HMDB51 (Kuehne et al., 2011). We use the same architecture and hyper-parameters; the only difference is the sampling approach.

	UCF101			HMDB51		
	$M=32$	$M=64$	$M=128$	$M=32$	$M=64$	$M=128$
Random	61.9	63.1	66.9	33.1	33.8	35.8
OHEM	50.2 (-11.7)	60.8 (-2.3)	65.7 (-1.2)	26.8 (-6.3)	30.1 (-3.7)	33.2 (-2.6)
Active	78.0 (+16.1)	78.9 (+15.8)	79.2 (+12.3)	41.2 (+8.1)	42.3 (+8.5)	42.6 (+6.8)

Table 5: Online hard example mining (OHEM) (Shrivastava et al., 2016) vs. our active sampling

Table 5 shows OHEM is generally less effective than both random sampling and our active sampling. Intuitively, OHEM promotes the dictionary to contain the most challenging keys for a given mini-batch of queries. Unfortunately, this causes OHEM to produce a *redundant* and *biased* dictionary, e.g., negative samples coming from a particular semantic category. This is shown in the table above: When M (mini-batch size) is small, the performance of OHEM is even worse than random sampling, although the gap between OHEM and random sampling decreases as M increases. We believe this is because OHEM has a higher chance of selecting similar negative instances. When M is large, this issue can be mitigated to some extent, but the performance still falls behind ours by a large margin. This suggests the importance of having a *diverse* set of negative samples, which is unique in our approach.

B WHEN WOULD CROSS-MODAL CONTRASTIVE LEARNING FAIL?

In general, cross-modal video representation learning is based on an assumption that the natural correspondence between audio and visual channels could serve as a useful source of supervision. While intuitive, this assumption may not hold for certain videos in-the-wild, which may cause the model to learn suboptimal representations. To investigate when our approach succeeds and fails, we conduct a post-hoc analysis by using the <https://www.overleaf.com/project/5ded2abe1c17bc00011e5da8> ground-truth semantic category labels provided in Kinetics-700 (Carreira et al., 2019) (which is not used during pretraining). Specifically, we use our pretrained model to solve the audio-visual contrastive pretext task (Eqn.(7) in the main paper) and keep track of the prediction results (correct/incorrect). We then average the pretext task accuracy over 100 randomly chosen samples for each action category.

Figure 4 shows the top-10 and bottom-5 classes by using both audio (left) and video (right) as the query. We observe that, the top ranked classes for both audio and video are the activities that have highly correlated visual-audio signals. For instance, `playing bass guitar`, `play piano`, and `play violin` are all activities related to music. The correlation of audio-visual signals for these activities are obvious; such highly correlated signals are easier to be learned in a cross-modal manner. On the contrary, the bottom ranked classes are those that have subtle audio-visual correlation, e.g. `tossing coin`, `shaking hand`, `looking at phone`, and `hugging`. We also investigate the distribution of hard-easy classes with that reported in Kinetics-700 (Carreira et al., 2019) learned by the I3D-RGB model (Carreira & Zisserman, 2017). Interestingly, we find that some hard classes (e.g. `karaoke` and `recording music`) are listed in our top ranked classes. We suspect that, when only learned within visual modality, some classes with cluttered or completed

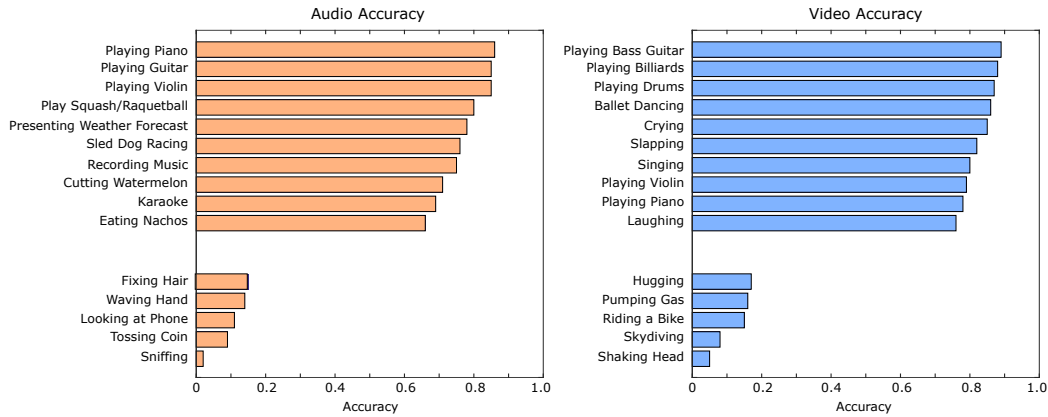


Figure 4: Distribution of Kinetics-700 (Carreira et al., 2019) categories sorted by the prediction accuracy.

spatial information will bring difficulties for classification. While, as our cross-modal approach can leverage information from both auditory and visual information, so our model does not limited by such problems.

C VISUALIZATION OF NEGATIVE INSTANCES

Figure 5 shows negative instances selected by random sampling and active sampling when we use audio clips as the query. We visualize the center frames of the selected video clips. We can see that our approach selects more **challenging** examples than the random sampling approach. For instance, given a query `opening bottle`, our approach selected video clips from the same or similar semantic categories, e.g. `drinking shot` and `opening bottle`. Given `snowboarding`, our approach selected more video clips related to categories containing the snow scene, e.g. `ice fishing`, `snow kiting`, and `tobogganing`.

Furthermore, we also find that our approach selects more **diverse** negative samples. For example, given a query `snowboarding`, active sampling selected video clips from 4 different categories related to the snow scene: (`ice fishing`, `playing ice hockey`, `snow kiting`, and `tobogganing`). In comparison, the random sampling approach yields fewer semantic categories in general. This suggests that our active sampling approach produces more ‘challenging’ and ‘diverse’ negative instances than the random sampling approach.

REFERENCES

- Humam Alwassel, Dhruv Mahajan, Lorenzo Torresani, Bernard Ghanem, and Du Tran. Self-supervised learning by cross-modal audio-video clustering. *arXiv preprint arXiv:1911.12667*, 2019.
- Relja Arandjelovic and Andrew Zisserman. Look, listen and learn. In *ICCV*, 2017.
- Relja Arandjelovic and Andrew Zisserman. Objects that sound. In *ECCV*, 2018.
- Sanjeev Arora, Hrishikesh Khandeparkar, Mikhail Khodak, Orestis Plevrakis, and Nikunj Saunshi. A theoretical analysis of contrastive unsupervised representation learning. In *ICML*, 2019.
- David Arthur and Sergei Vassilvitskii. K-means++: The advantages of careful seeding. In *SODA*, 2007.
- Yuki M Asano, Mandela Patrick, Christian Rupprecht, and Andrea Vedaldi. Labelling unlabelled videos from scratch with multi-modal self-supervision. *arXiv preprint arXiv:2006.13662*, 2020.

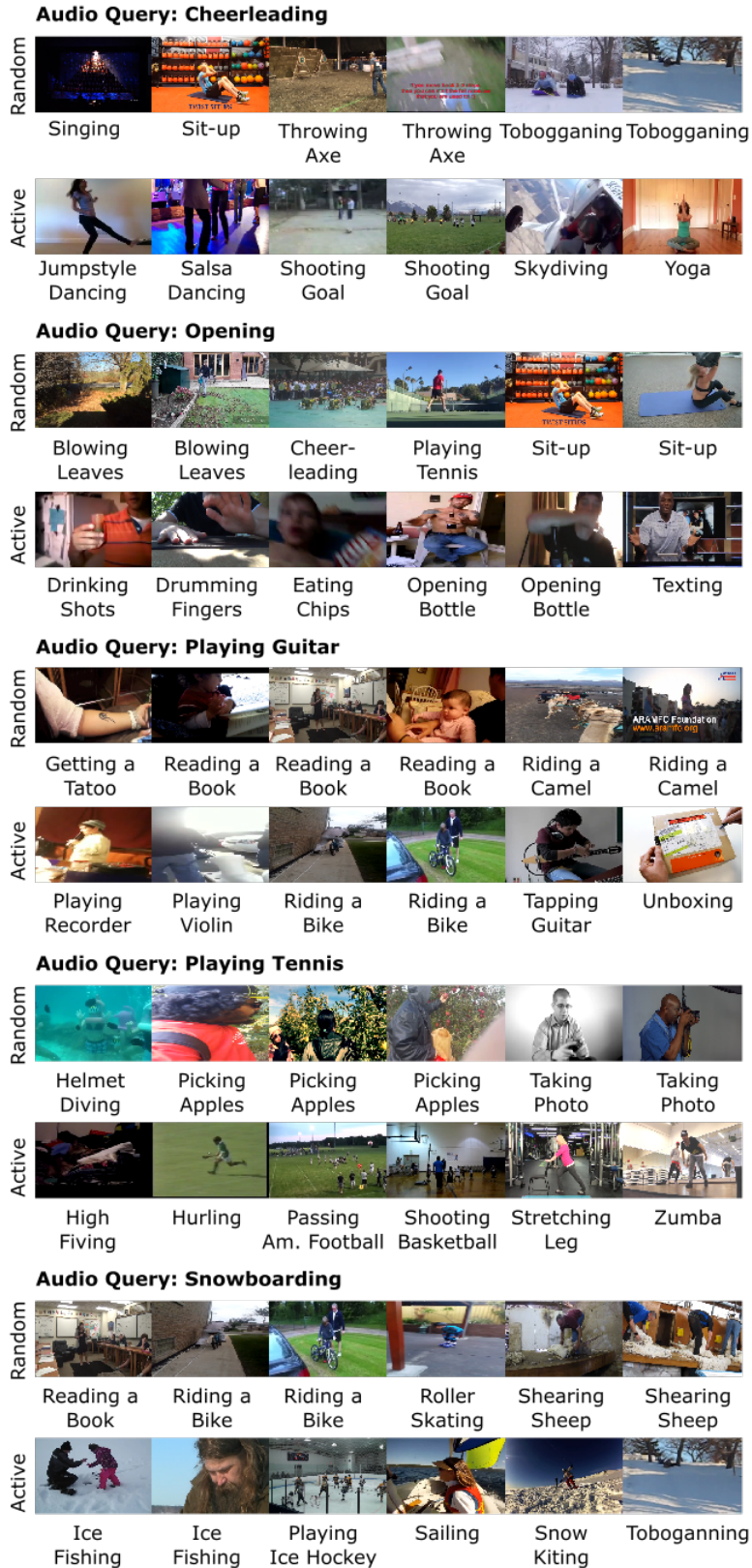


Figure 5: Center frames of video clips selected by random sampling and active sampling

Algorithm 2 Cross-Modal Contrastive Coding *without* Active Sampling

-
- 1: **Require:** Audio-visual clips A, V ; dictionary D_v ; encoders f_v, f_a, h_v, h_a ; dictionary size K ; mini-batch size M ; learning rate γ ; momentum m
 - 2: Initialize parameters, $\theta_q^v, \theta_k^v, \theta_q^a, \theta_k^a \sim \text{Uniform}(0, 1)$
 - 3: Load a dictionary at random, $D_a \leftarrow \{v_1, \dots, v_K\} \sim \text{Random}(V)$
 - 4: Load a dictionary at random, $D_v \leftarrow \{a_1, \dots, a_K\} \sim \text{Random}(A)$
 - 5: Encode dictionary samples, $k_i^v \leftarrow h_v(v_i), \forall v_i \in D_a, k_i^a \leftarrow h_a(a_i), \forall a_i \in D_v$
 - 6: **for** $epoch = 1$ **to** $\#epochs$: **do**
 - 7: **for** $t = 1$ **to** $\#mini\text{-batches}$: **do**
 - 8: Load a mini-batch of visual clips, $B_v \leftarrow \{v_1, \dots, v_M\} \sim V$
 - 9: Load a mini-batch of audio clips, $B_a \leftarrow \{a_1, \dots, a_M\} \sim A$
 - 10: \triangleright Update dictionaries
 - 11: Encode mini-batch samples, $k_i^v \leftarrow h_v(v_i), \forall v_i \in B_v$
 - 12: Encode mini-batch samples, $k_i^a \leftarrow h_a(a_i), \forall a_i \in B_a$
 - 13: Update $D_v \leftarrow \text{ENQUEUE}(\text{DEQUEUE}(D_v), B_v)$
 - 14: Update $D_a \leftarrow \text{ENQUEUE}(\text{DEQUEUE}(D_a), B_a)$
 - 15: \triangleright Cross-modal contrastive predictive coding
 - 16: Encode mini-batch samples, $q_i^v \leftarrow f_v(v_i), \forall v_i \in B_v$
 - 17: Encode mini-batch samples, $q_i^a \leftarrow f_a(a_i), \forall a_i \in B_a$
 - 18: Compute the posterior, $p(y_i^v | v_i, a_i, D_v) = \frac{\exp(q_i^v \cdot k_i^a / \tau)}{\sum_{j=0}^K \exp(q_i^v \cdot k_j^a / \tau)}, \forall i \in [1, M]$
 - 19: Compute the posterior, $p(y_i^a | a_i, v_i, D_v) = \frac{\exp(q_i^a \cdot k_i^v / \tau)}{\sum_{j=0}^K \exp(q_i^a \cdot k_j^v / \tau)}, \forall i \in [1, M]$
 - 20: \triangleright Update model parameters
 - 21: Update $\theta_q^v \leftarrow \theta_q^v - \gamma \nabla_{\theta} \mathcal{L}_{CE}(-\log p(y^v | \cdot), y_{gt}^v) |_{\theta=\theta_q^v}$
 - 22: Update $\theta_q^a \leftarrow \theta_q^a - \gamma \nabla_{\theta} \mathcal{L}_{CE}(-\log p(y^a | \cdot), y_{gt}^a) |_{\theta=\theta_q^a}$
 - 23: Momentum update $\theta_k^v \leftarrow m\theta_k^v + (1 - m)\theta_q^v$
 - 24: Momentum update $\theta_k^a \leftarrow m\theta_k^a + (1 - m)\theta_q^a$
 - 25: **end for**
 - 26: **end for**
 - 27: **return** Optimal solution $\theta_q^v, \theta_k^v, \theta_q^a, \theta_k^a$
-

Algorithm 3 k -MEANS_{INIT}⁺⁺ Seed Cluster Initialization

-
- 1: **Require:** Data X of N samples; number of centroids K
 - 2: Choose one centroid uniformly at random, $C[0] \leftarrow x \sim \text{Random}(X)$
 - 3: **for** $k = 1$ **to** $K - 1$: **do**
 - 4: \triangleright Compute a cumulative probability distribution with a probability in proportion to their squared distances from the nearest centroid that has already been chosen
 - 5: **for** $n = 0$ **to** $N - 1$: **do**
 - 6: Compute the squared distance, $D[n] \leftarrow (\text{min_dist}(X[n], C))^2$
 - 7: **end for**
 - 8: Compute the cumulative probability distribution, $P \leftarrow \frac{\text{cumsum}(D)}{\text{sum}(D)}$
 - 9: \triangleright The next centroid is chosen using $P(X)$ as a weighted probability distribution
 - 10: Choose one centroid at random, $C[k] \leftarrow x \sim P(X)$
 - 11: **end for**
 - 12: **return** C containing K centroids
-

- Jordan T Ash, Chicheng Zhang, Akshay Krishnamurthy, John Langford, and Alekh Agarwal. Deep batch active learning by diverse, uncertain gradient lower bounds. In *ICLR*, 2020.
- Yusuf Aytar, Carl Vondrick, and Antonio Torralba. Soundnet: Learning sound representations from unlabeled video. In *Advances in neural information processing systems*, 2016.
- Mohamed Ishmael Belghazi, Aristide Baratin, Sai Rajeshwar, Sherjil Ozair, Yoshua Bengio, Aaron Courville, and Devon Hjelm. Mutual information neural estimation. In *ICML*, 2018.
- Uta Buchler, Biagio Brattoli, and Bjorn Ommer. Improving spatiotemporal self-supervision by deep reinforcement learning. In *ECCV*, 2018.
- Joao Carreira and Andrew Zisserman. Quo vadis, action recognition? a new model and the kinetics dataset. In *CVPR*, 2017.
- Joao Carreira, Eric Noland, Chloe Hillier, and Andrew Zisserman. A short note on the kinetics-700 human action dataset. *arXiv preprint arXiv:1907.06987*, 2019.
- Ting Chen, Simon Kornblith, Mohammad Norouzi, and Geoffrey Hinton. A simple framework for contrastive learning of visual representations. In *ICML*, 2020.
- Jacob Devlin, Ming-Wei Chang, Kenton Lee, and Kristina Toutanova. BERT: Pre-training of deep bidirectional transformers for language understanding. In *ACL*, 2019.
- Debidatta Dwibedi, Yusuf Aytar, Jonathan Tompson, Pierre Sermanet, and Andrew Zisserman. Temporal cycle-consistency learning. In *CVPR*, 2019.
- Ariel Ephrat, Inbar Mosseri, Oran Lang, Tali Dekel, Kevin Wilson, Avinatan Hassidim, William T Freeman, and Michael Rubinstein. Looking to listen at the cocktail party: A speaker-independent audio-visual model for speech separation. *ACM Transactions on Graphics*, 2018.
- Fartash Faghri, David J Fleet, Jamie Ryan Kiros, and Sanja Fidler. VSE++: Improving visual-semantic embeddings with hard negatives. In *BMVC*, 2017.
- Satoru Fujishige. *Submodular functions and optimization*. 2005.
- Chuang Gan, Deng Huang, Hang Zhao, Joshua B Tenenbaum, and Antonio Torralba. Music gesture for visual sound separation. In *CVPR*, 2020.
- Ruohan Gao and Kristen Grauman. 2.5D visual sound. In *CVPR*, 2019a.
- Ruohan Gao and Kristen Grauman. Co-separating sounds of visual objects. In *ICCV*, 2019b.
- Ruohan Gao, Rogerio Feris, and Kristen Grauman. Learning to separate object sounds by watching unlabeled video. In *ECCV*, 2018.
- Jort F Gemmeke, Daniel PW Ellis, Dylan Freedman, Aren Jansen, Wade Lawrence, R Channing Moore, Manoj Plakal, and Marvin Ritter. Audio set: An ontology and human-labeled dataset for audio events. In *ICASSP*, 2017.
- Walter R Gilks, Sylvia Richardson, and David Spiegelhalter. *Markov chain Monte Carlo in practice*. Chapman and Hall/CRC, 1995.
- Michael Gutmann and Aapo Hyvärinen. Noise-contrastive estimation: A new estimation principle for unnormalized statistical models. In *AISTATS*, 2010.
- Tengda Han, Weidi Xie, and Andrew Zisserman. Video representation learning by dense predictive coding. In *ICCV*, 2019.
- Wangli Hao, Zhaoxiang Zhang, and He Guan. Cmcgan: A uniform framework for cross-modal visual-audio mutual generation. In *AAAI*, 2018.
- Kensho Hara, Hirokatsu Kataoka, and Yutaka Satoh. Can spatiotemporal 3d cnns retrace the history of 2d cnns and imagenet? In *CVPR*, 2018.

- Kaiming He, Xiangyu Zhang, Shaoqing Ren, and Jian Sun. Deep residual learning for image recognition. In *CVPR*, 2016.
- Kaiming He, Haoqi Fan, Yuxin Wu, Saining Xie, and Ross Girshick. Momentum contrast for unsupervised visual representation learning. In *CVPR*, 2020.
- Olivier J Hénaff, Ali Razavi, Carl Doersch, SM Eslami, and Aaron van den Oord. Data-efficient image recognition with contrastive predictive coding. *arXiv preprint arXiv:1905.09272*, 2019.
- R Devon Hjelm, Alex Fedorov, Samuel Lavoie-Marchildon, Karan Grewal, Phil Bachman, Adam Trischler, and Yoshua Bengio. Learning deep representations by mutual information estimation and maximization. In *ICLR*, 2018.
- Sergey Ioffe and Christian Szegedy. Batch normalization: Accelerating deep network training by reducing internal covariate shift. *arXiv preprint arXiv:1502.03167*, 2015.
- Longlong Jing and Yingli Tian. Self-supervised spatiotemporal feature learning by video geometric transformations. *arXiv preprint arXiv:1811.11387*, 2018.
- Will Kay, Joao Carreira, Karen Simonyan, Brian Zhang, Chloe Hillier, Sudheendra Vijayanarasimhan, Fabio Viola, Tim Green, Trevor Back, Paul Natsev, et al. The kinetics human action video dataset. *arXiv preprint arXiv:1705.06950*, 2017.
- Dahun Kim, Donghyeon Cho, and In So Kweon. Self-supervised video representation learning with space-time cubic puzzles. In *AAAI*, 2019.
- Diederik P Kingma and Jimmy Ba. Adam: A method for stochastic optimization. *arXiv preprint arXiv:1412.6980*, 2014.
- Bruno Korbar, Du Tran, and Lorenzo Torresani. Cooperative learning of audio and video models from self-supervised synchronization. In *Advances in Neural Information Processing Systems*, 2018.
- Hildegard Kuehne, Hueihan Jhuang, Estíbaliz Garrote, Tomaso Poggio, and Thomas Serre. Hmdb: a large video database for human motion recognition. In *ICCV*, 2011.
- Alex Kulesza and Ben Taskar. k-dpps: Fixed-size determinantal point processes. In *ICML*, 2011.
- Brenden M Lake, Ruslan Salakhutdinov, and Joshua B Tenenbaum. Human-level concept learning through probabilistic program induction. *Science*, 350(6266):1332–1338, 2015.
- Yann LeCun, Léon Bottou, Yoshua Bengio, and Patrick Haffner. Gradient-based learning applied to document recognition. *Proceedings of the IEEE*, 86(11), 1998.
- Hsin-Ying Lee, Jia-Bin Huang, Maneesh Singh, and Ming-Hsuan Yang. Unsupervised representation learning by sorting sequences. In *ICCV*, 2017.
- Gen Li, Nan Duan, Yuejian Fang, Ming Gong, Daxin Jiang, and Ming Zhou. Unicoder-vl: A universal encoder for vision and language by cross-modal pre-training. In *AAAI*, 2020.
- Liunian Harold Li, Mark Yatskar, Da Yin, Cho-Jui Hsieh, and Kai-Wei Chang. VisualBERT: A simple and performant baseline for vision and language. *arXiv preprint arXiv:1908.03557*, 2019.
- Yinhan Liu, Myle Ott, Naman Goyal, Jingfei Du, Mandar Joshi, Danqi Chen, Omer Levy, Mike Lewis, Luke Zettlemoyer, and Veselin Stoyanov. Roberta: A robustly optimized bert pretraining approach. *arXiv preprint arXiv:1907.11692*, 2019.
- Jiasen Lu, Dhruv Batra, Devi Parikh, and Stefan Lee. ViLBERT: Pretraining Task-Agnostic Visiolinguistic Representations for Vision-and-Language Tasks. In *Advances in neural information processing systems*, 2019.
- Odile Macchi. The coincidence approach to stochastic point processes. *Advances in Applied Probability*, 7(1), 1975.

- David McAllester and Karl Stratos. Formal limitations on the measurement of mutual information. In *AISTATS*, 2020.
- Ishan Misra, C. Lawrence Zitnick, and Martial Hebert. Shuffle and learn: Unsupervised learning using temporal order verification. In *ECCV*, 2016.
- Pedro Morgado, Nuno Vasconcelos, and Ishan Misra. Audio-visual instance discrimination with cross-modal agreement. *arXiv preprint arXiv:2004.12943*, 2020.
- Hyeonseob Nam and Bohyung Han. Learning multi-domain convolutional neural networks for visual tracking. In *CVPR*, 2016.
- George L Nemhauser, Laurence A Wolsey, and Marshall L Fisher. An analysis of approximations for maximizing submodular set functions. *Mathematical programming*, 14(1), 1978.
- Aaron van den Oord, Yazhe Li, and Oriol Vinyals. Representation learning with contrastive predictive coding. *arXiv preprint arXiv:1807.03748*, 2018.
- Andrew Owens and Alexei A Efros. Audio-visual scene analysis with self-supervised multisensory features. In *ECCV*, 2018.
- Andrew Owens, Jiajun Wu, Josh H McDermott, William T Freeman, and Antonio Torralba. Ambient sound provides supervision for visual learning. In *ECCV*, 2016.
- Sherjil Ozair, Corey Lynch, Yoshua Bengio, Aaron Van den Oord, Sergey Levine, and Pierre Sermanet. Wasserstein dependency measure for representation learning. In *Advances in Neural Information Processing Systems*, 2019.
- Jiangmiao Pang, Kai Chen, Jianping Shi, Huajun Feng, Wanli Ouyang, and Dahua Lin. Libra R-CNN: Towards balanced learning for object detection. In *CVPR*, 2019.
- Mandela Patrick, Yuki M Asano, Ruth Fong, João F Henriques, Geoffrey Zweig, and Andrea Vedaldi. Multi-modal self-supervision from generalized data transformations. *arXiv preprint arXiv:2003.04298*, 2020.
- Karol J Piczak. Environmental sound classification with convolutional neural networks. In *International Workshop on Machine Learning for Signal Processing (MLSP)*, 2015a.
- Karol J Piczak. ESC: Dataset for environmental sound classification. In *Proceedings of the 23rd ACM international conference on Multimedia*, 2015b.
- Hardik B Sailor, Dharmesh M Agrawal, and Hemant A Patil. Unsupervised filterbank learning using convolutional restricted boltzmann machine for environmental sound classification. In *INTERSPEECH*, 2017.
- Steffen Schneider, Alexei Baevski, Ronan Collobert, and Michael Auli. wav2vec: Unsupervised pre-training for speech recognition. *arXiv preprint arXiv:1904.05862*, 2019.
- Pierre Sermanet, Corey Lynch, Jasmine Hsu, and Sergey Levine. Time-contrastive networks: Self-supervised learning from multi-view observation. In *CVPRW*, 2017.
- Burr Settles. Active learning literature survey. Technical report, University of Wisconsin-Madison Department of Computer Sciences, 2009.
- Abhinav Shrivastava, Abhinav Gupta, and Ross Girshick. Training region-based object detectors with online hard example mining. In *CVPR*, 2016.
- Khurram Soomro, Amir Roshan Zamir, and Mubarak Shah. Ucf101: A dataset of 101 human actions classes from videos in the wild. *arXiv preprint arXiv:1212.0402*, 2012.
- Weijie Su, Xizhou Zhu, Yue Cao, Bin Li, Lewei Lu, Furu Wei, and Jifeng Dai. Vi-bert: Pre-training of generic visual-linguistic representations. *arXiv preprint arXiv:1908.08530*, 2019.
- Chen Sun, Fabien Baradel, Kevin Murphy, and Cordelia Schmid. Contrastive bidirectional transformer for temporal representation learning. *arXiv preprint arXiv:1906.05743*, 2019a.

- Chen Sun, Austin Myers, Carl Vondrick, Kevin Murphy, and Cordelia Schmid. Videobert: A joint model for video and language representation learning. In *ICCV*, 2019b.
- Hao Tan and Mohit Bansal. LXMERT: Learning cross-modality encoder representations from transformers. *arXiv preprint arXiv:1908.07490*, 2019.
- Jiangliu Wang, Jianbo Jiao, Linchao Bao, Shengfeng He, Yunhui Liu, and Wei Liu. Self-supervised spatio-temporal representation learning for videos by predicting motion and appearance statistics. In *CVPR*, 2019a.
- Xiaolong Wang, Allan Jabri, and Alexei A Efros. Learning correspondence from the cycle-consistency of time. In *CVPR*, 2019b.
- Dejing Xu, Jun Xiao, Zhou Zhao, Jian Shao, Di Xie, and Yueting Zhuang. Self-supervised spatiotemporal learning via video clip order prediction. In *CVPR*, 2019.
- Karren Yang, Bryan Russell, and Justin Salamon. Telling left from right: Learning spatial correspondence of sight and sound. In *CVPR*, 2020.
- Zhilin Yang, Zihang Dai, Yiming Yang, Jaime Carbonell, Russ R Salakhutdinov, and Quoc V Le. Xlnet: Generalized autoregressive pretraining for language understanding. In *Advances in neural information processing systems*, 2019.
- Hang Zhao, Chuang Gan, Andrew Rouditchenko, Carl Vondrick, Josh McDermott, and Antonio Torralba. The sound of pixels. In *ECCV*, 2018.
- Hang Zhao, Chuang Gan, Wei-Chiu Ma, and Antonio Torralba. The sound of motions. In *ICCV*, 2019.
- Yipin Zhou, Zhaowen Wang, Chen Fang, Trung Bui, and Tamara L Berg. Visual to sound: Generating natural sound for videos in the wild. In *CVPR*, 2018.